Random Effects in a Nonlinear Vibration-Based Piezoelectric Energy Harvesting System

Tiago Leite Pereira[*], Aline Souza de Paula[†]
and Adriano Todorovic Fabro[‡]
*Department of Mechanical Engineering,
Universidade de Brasília,
70.910-900, Brasília, DF, Brazil*
*tiagolei.tl@gmail.com
†alinedepaula@unb.br
‡fabro@unb.br*

Marcelo Amorim Savi
*COPPE/Department of Mechanical Engineering,
Universidade Federal do Rio de Janeiro,
Center for Nonlinear Mechanics,
21.941.972, Rio de Janeiro – RJ,
P. O. Box 68.503, Brazil*
savi@mecanica.ufrj.br

Vibration-based energy harvesting is of increasing importance and there is a current challenge to improve energy harvesting capacity exploiting nonlinear and random effects. This article investigates random effects in a nonlinear energy harvesting system. The system is represented by a magnetoelastic structure with two piezoceramic layers attached to the root of a cantilever beam, obtaining a bimorph generator. The energy harvesting system is subjected to three excitation conditions: pure harmonic, pure random and a combination of harmonic and random excitations. Noise-to-Signal Ratio (NSR) is employed to quantify different combinations of the forcing terms, establishing a procedure to evaluate the system performance. This approach is based on Power Spectral Density (PSD) of input and output signals. Numerical simulations are carried out, identifying the better combinations of harmonic and random excitations for energy harvesting purposes. Discussions about the influence of the kind of response are carried out evaluating the differences between periodic and chaotic motions. Conclusions show that both random and nonlinear effects can be tuned in order to enhance energy harvesting capacity.

Keywords: Piezoelectric; nonlinear dynamics; energy harvesting; randomness; chaotic response; bifurcation.

1. Introduction

Piezoelectric vibration-based energy harvesting is of increasing importance due to the necessity of clean energy generation. Besides that, it can be used together with vibration reduction purpose, creating a dynamical absorber that will be useful for either energy harvesting or vibration reduction. The current challenge is the energy harvesting enhancement that motivates the analysis of nonlinear and random effects.

Several applications have been analyzed through different research efforts. The use of human

walk movement is an interesting possibility to charge portable electronic devices using ambient vibration. In this regard, Feenstra *et al.* [2008] and Rome *et al.* [2005] investigated a system that can be used in backpack. Shenck and Paradiso [2001] proposed a device to be used in shoes. Sohn *et al.* [2005] proposed an energy harvesting device to be applied to the blood pressure variation. Hou *et al.* [2017] developed a sensor to monitor a pavement powered by the energy provided by a piezoelectric cantilever beam.

The analysis of linear energy harvesting devices shows that an excitation close to the system resonant condition is the best option to obtain a reasonable amount of generated energy. Nevertheless, small variations from this resonant condition cause drastic reduction of the electrical response, making the linear system to be narrowband vibration energy harvesting. Broadband vibration in linear energy harvesters can be obtained by considering self-tuned systems using active or semi-active control [Cheng *et al.*, 2017; Lallart *et al.*, 2010; Roundy & Zhang, 2005].

Based on that, nonlinear systems are imagined in order to spread the energy to a broadband energy harvester. The increase of the number of equilibrium points is an interesting possibility related to the introduction of nonlinear effects on energy harvesting systems. Basically, the introduction of new equilibrium points can be exploited forcing the system to oscillate around more points, increasing the motion amplitudes and therefore, the energy harvested. In this regard, bistable or tristable oscillators are exploited.

Concerning bistable systems, Litak *et al.* [2016] investigated a vertical beam with a tip mass. Kim *et al.* [2016] showed that out-of-phase mode is the best regime, under resonant conditions, for energy harvesting purpose. Chiacchiari *et al.* [2017] investigated the harvested energy in a bistable system subjected to impulsive excitations. Some authors explored magnetic interaction to obtain a bistable system, as investigated by Mann and Sims [2009], Erturk *et al.* [2009] and Abdelmoula *et al.* [2017].

Concerning tristable systems, Zhou *et al.* [2016] analyzed the external load influence. Oumbé Tékam *et al.* [2015] used the Melnikov criterion to analyze complex dynamics. Similar system was explored by Cao *et al.* [2015] showing the influence of geometry parameters. Zhou *et al.* [2015] addressed a system that can be bistable or tristable by shifting some

parameters, with impact-induced device. Results showed that the system obtains high energy oscillations under low excitation levels.

Silva *et al.* [2015] investigated the influence of nonlinear piezoelectric couplings indicating that quadratic constitutive equations can strongly modify the system dynamics, presenting better matches with experimental data. Triplett and Quinn [2009] showed that nonlinearities of the piezoelectric coupling can enhance the harvested energy, however, the efficiency of the system can be reduced. Silva *et al.* [2013] analyzed hysteretic piezoelectric behavior suggesting that optimum responses can be found depending on the hysteresis level.

The analysis of random effects is another important aspect to be evaluated concerning energy harvesting capacity enhancement. Basically, energy due to nondeterministic sources can alter system response, changing system capacity. Leng *et al.* [2017] investigated the performance of a tristable piezoelectric energy harvester under random excitation. Litak *et al.* [2010] verified that a bistable structure has a stochastic resonance when excited with a white noise excitation. De Paula *et al.* [2015] investigated a system subjected to a random excitation establishing a comparison among linear, nonlinear monostable and nonlinear bistable configurations. Results showed conditions where random excitation influenced system performance. Ferrari *et al.* [2011] evaluated RMS voltage on bistable system.

In general, it is possible to say that the combination of random and nonlinear effects seems to be an essential point to be exploited in vibration-based energy harvesting systems. Besides, the presence of noise is unavoidable in experimental systems, meaning that the influence of randomness on deterministic systems needs to be considered for design purposes [Litak, 2014].

This paper investigates the influence of randomness on nonlinear energy harvesting system. A bistable piezomagnetoelastic structure subjected to deterministic and nondeterministic excitations is analyzed. Basically, three excitation conditions are treated: a pure harmonic; a pure random; and random-harmonic combination. Energy harvesting system performance is evaluated by proposing a procedure based on Power Spectral Density (PSD) that uses information of input (mechanical excitation) and output (voltage). Results show that both effects can alter energy harvesting capacity and need to be explored for enhancement purposes.

Numerical simulations are carried out identifying the better combinations of harmonic and random excitations for energy harvesting purposes.

After this introduction, this paper is organized as follows. In Sec. 2, the mathematical model of the piezomagnetoelastic structure is presented, proposing a procedure to evaluate system performance appropriate for both deterministic and nondeterministic signals. In Sec. 3, numerical simulations are carried out considering harmonic excitation, while in Sec. 4, random excitation is of concern. Combined harmonic and random excitations are treated in the sequence. Section 5 presents the system dynamical behavior, evaluating different noise levels. Section 6 discusses system performance. Finally, the concluding remarks are discussed.

2. Piezomagnetoelastic Structure

Consider an energy harvesting system represented by a magnetoelastic structure that captures the environmental vibration using piezoelectric elements. Figure 1 presents a schematic representation of the structure that consists of a ferromagnetic cantilever beam with two permanent magnets, one located at the free end of the beam and the other at a vertical distance d from free end. The mechanical system is based on [Moon & Holmes, 1979] presenting a Duffing-type nonlinearity. The use of this device as an energy harvester is associated with piezoelectric elements that perform electric-mechanical coupling. Erturk *et al.* [2009] used two piezoceramic layers to the cantilever beam root obtaining a bimorph generator. The piezoelectric layers are connected to an electrical circuit that, for the sake of simplicity, can be represented by a
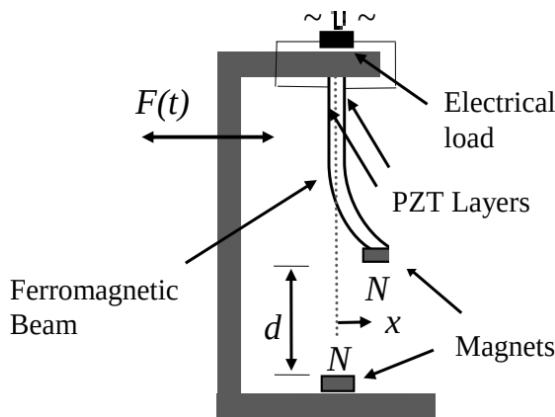

Fig. 1.   Schematic representation of the piezomagnetoelastic structure.

resistor. Base excitation is represented by a combination of random and harmonic excitations considering three situations: pure harmonic; pure random; harmonic and random combination.

Equations of motion of the energy harvesting system are presented in the sequence assuming that x is the dimensionless transverse direction tip displacement of the beam and v is the dimensionless voltage across the load resistance. Time, t, is also dimensionless as considered by Moon and Holmes [1979] and Erturk *et al.* [2009]. By assuming a linear electro-mechanical piezoelectric coupling, governing equations are the following,

$$\ddot{x} + 2\xi\dot{x} - \frac{1}{2}x(1 - x^2) - \chi v = F(t), \qquad (1)$$

$$\dot{v} + \lambda v + \kappa\dot{x} = 0, \qquad (2)$$

where ξ is the mechanical damping ratio, χ is the dimensionless piezoelectric coupling term in the mechanical equation, κ is the dimensionless piezoelectric coupling term in the electrical circuit equation, λ is the reciprocal of the dimensionless time constant ($\lambda \propto 1/R_L C_P$ where R_L is the load resistance and C_P is the equivalent capacitance of the piezoceramic layers) and $F(t)$ is the dimensionless excitation due to base movement. It is important to highlight that the system is dimensionless, this process can be seen in the works of Moon and Holmes [1979] and Erturk *et al.* [2009].

System parameter values are the same as considered by Erturk *et al.* [2009]: $\xi = 0.01$, $\chi = 0.05$, $\kappa = 0.5$ and $\lambda = 0.05$. Under these assumptions, the equilibrium points of the structure are composed by two stable spiral points located at $(x, \dot{x}, v) = (\pm 1, 0, 0)$ and unstable saddle point located at $(x, \dot{x}, v) = (0, 0, 0)$, characterizing a typical bistable system.

Three different excitations, $F(t)$, are treated considering a combination of random and harmonic situations. In the first case, a pure harmonic excitation is considered, $F(t) = f_0 \cos(\omega t)$ where f_0 is the dimensionless excitation amplitude due to base movement ($f_0 \propto \Omega^2 X_0$ where X_0 is the dimensionless base displacement amplitude). In the second case, a random excitation is considered, $F(t) = N(\sigma, \bar{x})$ representing a Gaussian white noise with mean value $\bar{x}$ and standard-deviation σ. Finally, a combined harmonic and random forcing excitation is treated. The general case is represented as follows,

$$F(t) = f_0 \cos(\omega t) + N(\sigma, \bar{x}). \qquad (3)$$

In order to characterize the combination of random and harmonic excitations, Noise-to-Signal Ratio (NSR) measure is established

$$\text{NSR} = \frac{\sigma}{f_0}. \tag{4}$$

2.1. *Energy harvesting and system performance*

The energy harvesting system has a performance related to electro-mechanical conversion. In brief, it is important to establish a relation between mechanical, or input, and electrical, or output, responses. The combination of harmonic and random excitations is important to establish a proper criterion for this aim. An interesting possibility to analyze energy harvesting capacity proposed in this article is based on the Power Spectral Density (PSD). The PSD is the power distribution in frequency domain, defined as follows:

$$\text{PSD} = \frac{|\hat{x}(\hat{\omega})|^2}{T}, \tag{5}$$

where $\hat{x}(\hat{\omega})$ is the Fourier Transform of $x(t)$, $\hat{\omega}$ are frequencies that construct the analyzed signal

$$\hat{x}(\hat{\omega}) = \int_{-\infty}^{\infty} e^{-2\pi i \hat{\omega} t} x(t) dt \tag{6}$$

and T is the total time of analysis. The area under the curve of PSD is defined as Power of the Signal (PS). Moreover, it is important to define the PS of the excitation (PS_f) and voltage (PS_v). The relation between these two quantities, r, is an indicator of the system performance, as first proposed by Pereira *et al.* [2017], that presents a preliminary analysis of the system studied in the present work:

$$r = \frac{\int_0^{\hat{\omega}_u} \text{PSD}_v(\hat{\omega}) d\hat{\omega}}{\int_0^{\hat{\omega}_u} \text{PSD}_f(\hat{\omega}) d\hat{\omega}} = \frac{\text{PS}_v}{\text{PS}_f}. \tag{7}$$

The value of PSD_f is the mechanical input power decomposed in the frequency domain representing a measure of the mechanical energy. On the other hand, the value of PSD_v is the electrical output power decomposed in the frequency domain related to the electrical output representing a measure of the harvested energy. They are both calculated by an FFT-based periodogram approach

and Hanning windowing [Newland, 1993]. Based on that, PS_v and r are parameters used to evaluate the harvested energy and system performance, respectively. Since the quantities $v(t)$ and $F(t)$ are dimensionless, PS_v and PS_f can be compared directly. The values of ratio r can be greater than 1 meaning that the area under PSD of electrical output is greater than the area related to PSD of mechanical input. Besides, the ratio r is evaluated from 0 up to $\hat{\omega}_u$, within the frequency band of interest. This procedure is appropriate for both deterministic and nondeterministic signals.

3. Harmonic Excitation

This section discusses the energy harvesting system subjected to pure harmonic excitation. Initially, Fig. 2(a) shows the basin of attraction for $\omega = 0.8$ and $f_0 = 0.083$, where two coexistent attractors are observed. The black points are associated with initial conditions that lead to a period-1 attractor, shown in phase space and Poincaré section in Fig. 2(b), while white points are initial conditions associated with a chaotic behavior in steady state. The chaotic response is presented in phase space and Poincaré section in Figs. 2(c) and 2(d), respectively. All Poincaré sections presented in this work are constructed based on the forcing frequency, when forcing phase is equal to zero.

Based on the two behaviors identified in Fig. 2, system response is evaluated for different forcing parameter. At first, Fig. 3 shows the qualitative change of system response from bifurcation diagrams by varying forcing parameters, either amplitude or frequency. When the forcing amplitude is varied [Fig. 3(a)], a constant frequency $\omega = 0.8$ is considered. In addition, when the forcing frequency is under variation, a constant forcing amplitude $f_0 = 0.083$ is applied. Two different initial conditions are treated. The black points are associated with initial conditions $(x_0, \dot{x}_0, v_0) = (1, 0, 0)$, which correspond to a chaotic response for the initial forcing parameters considered, while the pink points are associated with initial condition $(x_0, \dot{x}_0, v_0) = (1, 1, 0)$, which corresponds to a period-1 orbit for the initial forcing parameters. Note that these initial values of f_0 and ω are in the middle of the bifurcation diagrams presented in Figs. 3(a) and 3(b). From the two reference behaviors, chaotic and period-1 orbits, forcing amplitude is increased and decreased and plotted together in the diagram
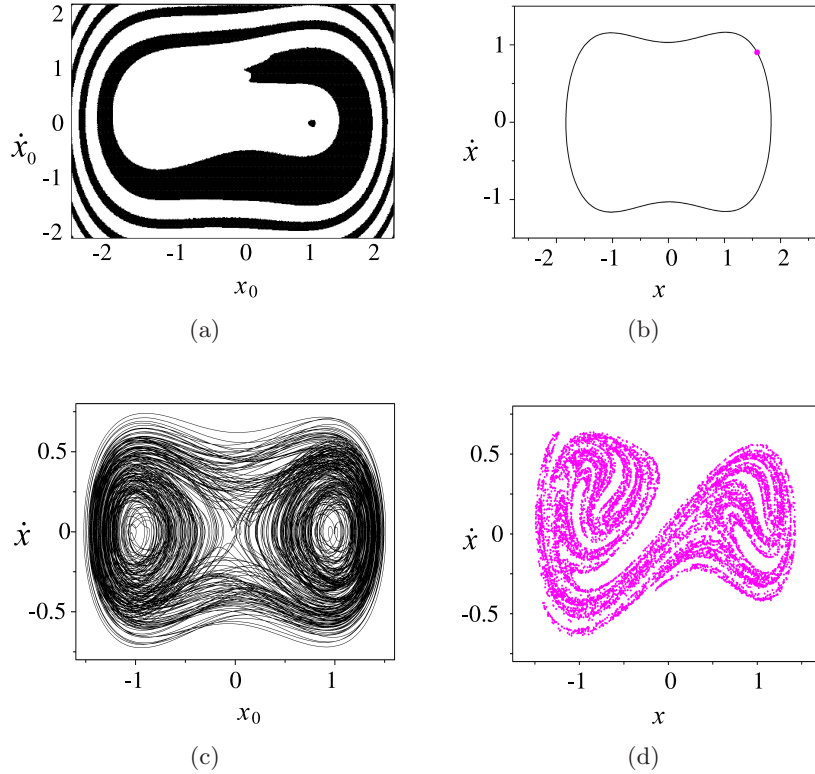
Fig. 2. System behavior for $\omega = 0.8$ and $f_0 = 0.083$: (a) Basin of attraction; (b) period-1 attractor associated with the black points of the basin of attraction in phase space and Poincaré section; chaotic response associated with the white points of the basin of attraction in (c) phase space and (d) Poincaré section.

of Fig. 3(a). A similar procedure is adopted for forcing frequency and is shown in Fig. 3(b). From the initial period-1 orbit (pink points), only periodic behaviors are observed when varying forcing amplitude and frequency. When starting from the chaotic response (black points), different kinds of responses are observed, including periodic behavior with different periodicity and chaotic response. By considering black and pink points of both bifurcation diagrams, coexisting attractors are observed in Fig. 3(a) for values of f_0 greater than 0.03 and in

Fig. 3(b) for values of ω greater than 0.27. In the forthcoming analysis, nine different responses are chosen to be further investigated.

Based on the global analysis provided by the bifurcation diagrams, different kinds of responses are picked to analyze the system performance. Table 1 identifies and classifies some responses, presenting forcing parameters and initial conditions. Note that the phase space and Poincaré section consist in a three-dimensional space $(x, \dot{x}, v)$, however, only the projection in the space of $(x, \dot{x})$ is
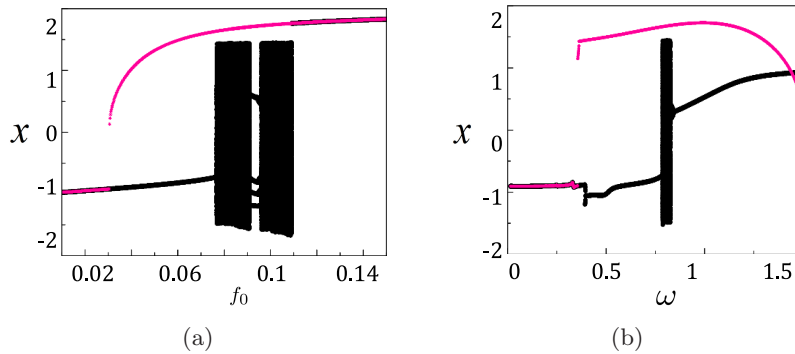

Fig. 3. Bifurcation diagram: (a) $\omega = 0.8$ and different values of f_0 and (b) $f_0 = 0.083$ and different values of ω. Chaotic (black) and period-1 orbits (pink).

Table 1.   Forcing parameters and initial condition.

	ω	f_0	Initial Condition	Behavior
Case 1	0.500	0.100	$(1.426, 0.480, -0.726)$	*Periodic*
Case 2	0.800	0.083	$(1.000, 1.000, 0.000)$	*Periodic*
Case 3	1.400	0.100	$(0.960, 2.966, -0.519)$	*Periodic*
Case 4	0.800	0.083	$(1.000, 0.000, 0.000)$	*Chaotic*
Case 5	0.800	0.100	$(-1.231, -0.004, 0.347)$	*Chaotic*
Case 6	0.865	0.100	$(-0.672, 0.283, -0.178)$	*Chaotic*
Case 7	0.800	0.093	$(-1.000, 0.000, 0.000)$	*Periodic*
Case 8	0.815	0.100	$(0.298, 0.419, -0.518)$	*Periodic*
Case 9	0.800	0.063	$(1.173, -0.002, -0.099)$	*Chaotic*

presented. Cases 1 to 3 are period-1 responses and their phase space and Poincaré section are shown in Fig. 4(a). Cases 4 to 6 are chaotic presenting phase space and Poincaré section in Figs. 4(b)–4(d). Cases 7 and 8 are period-5 responses shown in Fig. 4(e). Case 9 is presented in Fig. 4(f), being associated with a period-1 orbit that oscillates around only one equilibrium point $(1, 0, 0)$, different from Cases 1–3 that oscillate around both stable equilibrium points. The system evolves to this oscillatory behavior around the equilibrium point $(1, 0, 0)$ due to the initial condition. Note that
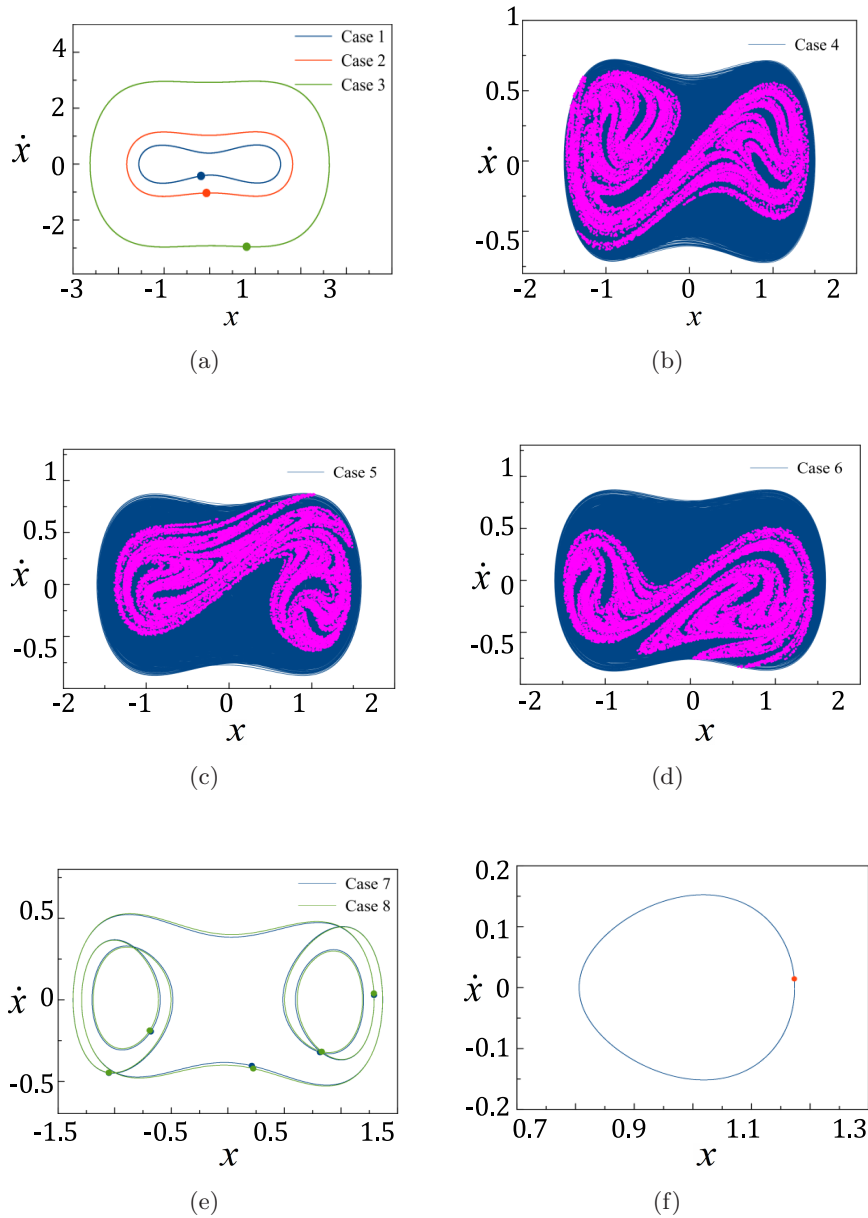

Fig. 4.   Phase space (line) and Poincaré section (point): (a) Cases 1–3, (b) Case 4, (c) Case 5, (d) Case 6, (e) Cases 7–8 and (f) Case 9.

equilibrium point $(-1, 0, 0)$ remains stable, thus, due to the symmetry of the system, depending on the initial conditions, system trajectory leads to an orbit symmetric to the one presented in Case 9 that oscillates around $(-1, 0, 0)$. It should be observed that Cases 2 and 4 are coexisting behaviors. In general, it is possible to establish four qualitatively different kinds of behaviors: period-1 oscillating around two stable equilibrium points (SEP), chaotic, period-5 and period-1 oscillating around only one SEP.

In order to investigate the frequency domain response, Fig. 5 shows the distribution of power of input signal (PSD_f), mechanical displacement (PSD_x) and electric output (PSD_v). Figure 5(a) presents the spectrum of the period-1 response oscillating around two SEP (Case 2), showing a discrete number of peaks that is a characteristic of a periodic signal. Note that similar behavior is presented with the greatest peak occurring in the same frequency of peak. Chaotic response spectrum (Case 4) is

presented in Fig. 5(b) showing a distribution of the power around a broad band of frequency. Period-5 response spectrum (Case 7) is presented in Fig. 5(c) showing more peaks when compared to Case 2, representing that more frequencies are present in the response. The spectrum of period-1 response oscillating around only one SEP (Case 9) is presented in Fig. 5(d) showing the presence of a discrete number of peaks with the first peak of response in the same frequency of the excitation peak, as observed in Case 2 analysis.

Frequency domain analysis of all cases are assessed and summarized in Table 2. Values are presented for PS_V, PS_f and ratio r. Cases 1 to 3 are related to period-1 orbits that oscillate around multiple SEP but with different amplitudes. Note that higher amplitudes are associated with higher values of PS_v. Thus, the oscillation amplitude is directly related to the harvested energy and Case 3 presents the best results. Case 3 also presents the best performance, and greater value of r, since variation of
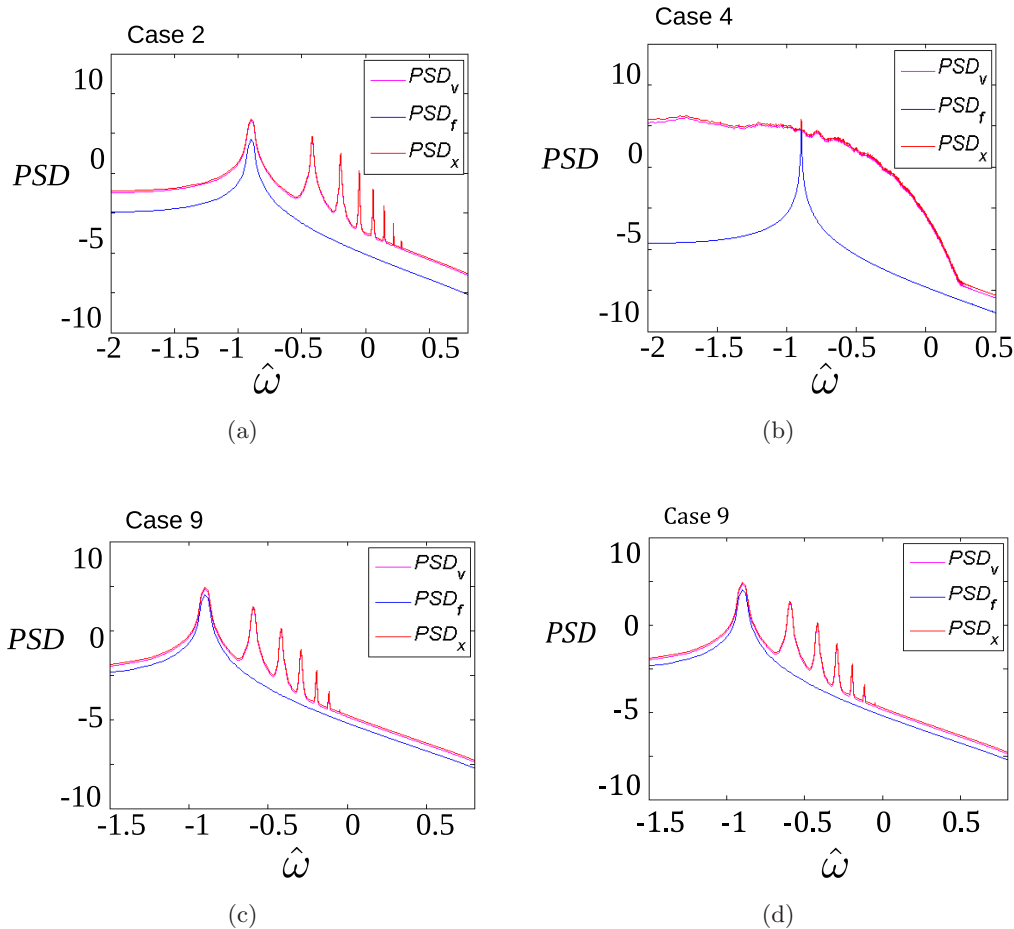

Fig. 5.   PSD curves for (a) Case 2, (b) Case 4, (c) Case 7 and (d) Case 9.

Table 2. Forcing parameters and initial condition.

	Behavior	$PS_f (10^{-3})$	$PS_v (10^{-3})$	r
Case 1	*Periodic*	0.10	11.09	110.96
Case 2	*Periodic*	0.68	17.81	258.53
Case 3	*Periodic*	0.10	39.31	393.13
Case 4	*Chaotic*	0.68	7.36	106.87
Case 5	*Chaotic*	1.00	7.96	79.60
Case 6	*Chaotic*	1.00	7.60	76.01
Case 7	*Periodic*	0.86	9.30	107.59
Case 8	*Periodic*	1.00	9.43	94.33
Case 9	*Chaotic*	0.39	0.19	4.83

PS_f values are considerably smaller than variation of PS_v.

Cases 4 to 6 are related to the chaotic behavior. From phase spaces [Figs. 4(b)–4(d)], it is observed that the system trajectory fills all phase space and oscillation amplitudes are similar. This similarity leads to similar values of PS_v. The best case is obtained from the greatest value of r, which is related to Case 4.

Cases 7 and 8 present period-5 orbits, as shown in the Poincaré section of Fig. 4(e). The two orbits are similar and, therefore, the values of PS_v are very

close. In contrast, the value of r is greatest in Case 7, indicating the best performance.

Case 9 presents the lowest values of PS_v and r of all cases. This is expected since this orbit has an oscillatory response around only one SEP, presenting small amplitudes [Fig. 4(f)].

Based on this analysis, one can conclude that the best orbit for energy harvesting purpose is related to higher oscillation amplitudes, represented by Case 3. When comparing chaotic behavior (Cases 4–6) with a periodic one that presents similar vibration amplitude (Case 1), the periodic solution presents the highest value of PS_v, being more appropriate for energy harvesting. This happens because the periodic solution always presents the highest amplitude while the chaotic solution visits distinct unstable orbits with different amplitudes.

4. Random Excitation

This section analyzes the energy harvesting system subjected to white noise excitation for different values of excitation variance. Figure 6 presents three different excitation characteristics, presenting
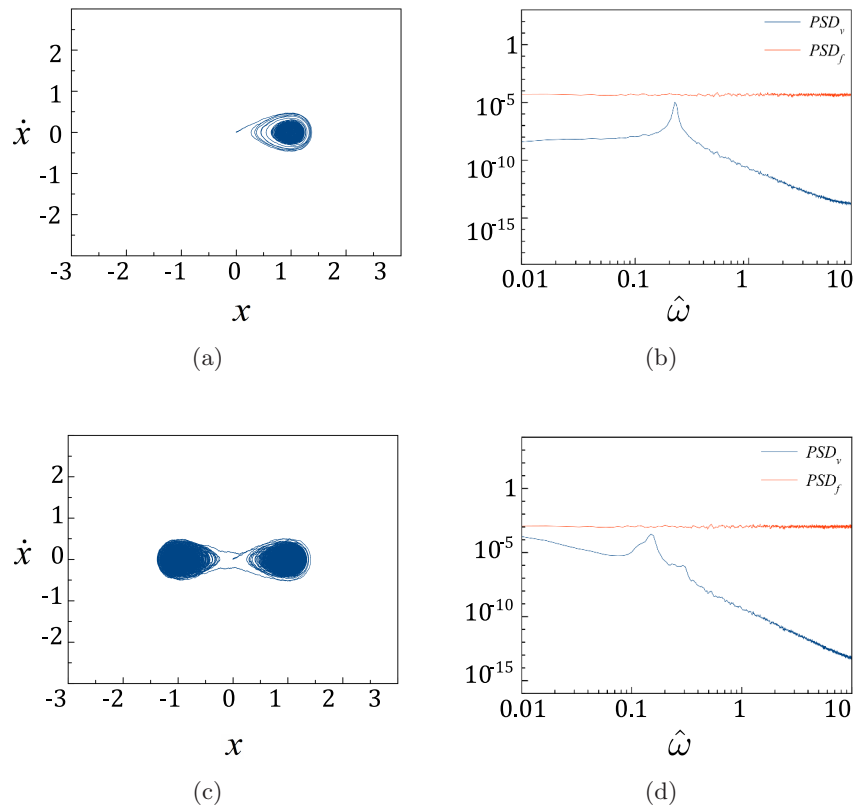

Fig. 6. Response in time domain and the PSD curve for (a) and (b) $\sigma = 0.2$, (c) and (d) $\sigma = 0.4$ and (e) and (f) $\sigma = 2$.
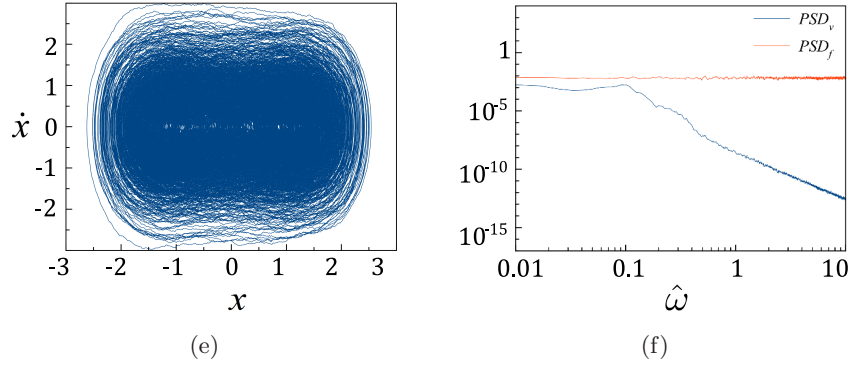
(e)

(f)

Fig. 6.   (*Continued*)

phase space, as well as PSD_f and PSD_v: $\sigma = 0.2$, Figs. 6(a) and 6(b); $\sigma = 0.4$, Figs. 6(c) and 6(d); and $\sigma = 2$, Figs. 6(e) and 6(f). It is noticeable from Fig. 6(a) that for $\sigma = 0.2$ the system visits only one SEP, and therefore, presents small amplitude. By increasing the variance to $\sigma = 0.4$ [Fig. 6(c)], the system starts to visits multiple SEP, as can be observed from system response around $x = -1$ and $x = +1$. For $\sigma = 2$, the system oscillates around multiple SEP with more transitions between them when compared to the lower variance of $\sigma = 0.4$.

It has been experimentally verified that energy harvesting system subjected to random excitation presents greater output voltage values when the beam oscillates around multiple SEP. Moreover, the best performance is obtained when a greater number of transitions from one SEP to the other occurs [De Paula *et al.*, 2015].

Table 3 presents the results of harvested energy and system performance of all cases analyzed under random excitation. Figure 7 summarizes the same results highlighting the kinds of response, presenting PS_f, PS_v and r, as a function of excitation

Table 3.   Harvested energy and system performance of cases analyzed under random excitation.

σ	$\text{PS}_f(10^{-3})$	$\text{PS}_v(10^{-3})$	r
0.2	0.80	0.03	0.3722
0.4	3.22	0.19	0.0588
0.6	7.25	0.86	0.1184
0.8	12.90	1.52	0.1177
1.0	20.16	1.90	0.0942
1.2	29.03	3.28	0.1129
1.4	39.52	3.69	0.0933
1.6	51.62	4.13	0.0800
1.8	65.33	4.17	0.0638
2.0	80.66	5.67	0.07025

(a)

(b)

(c)
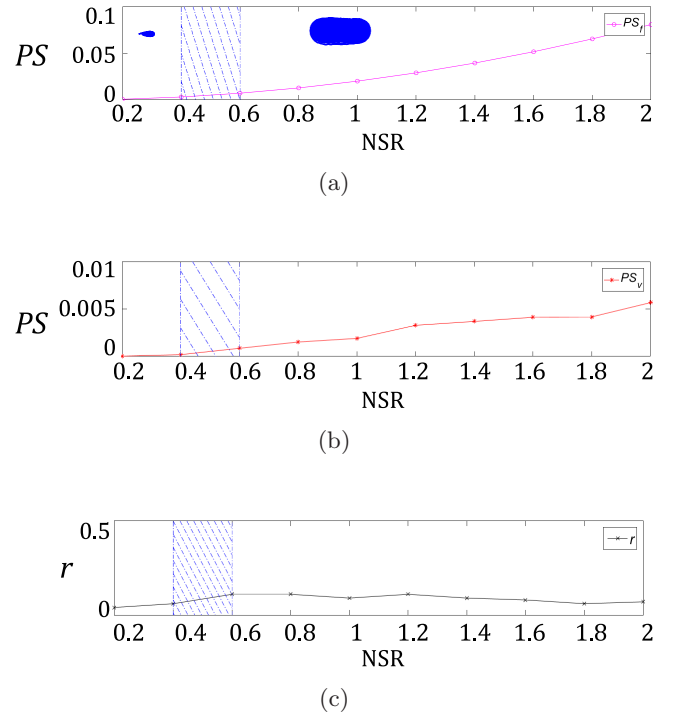
Fig. 7.   System behavior when σ is increased from 0.2 to 2: (a) PS_f and qualitative response of the system identified in phase space, (b) PS_v and (c) r.

variance, σ, varied from 0.2 to 2. The variance is related with the signal dispersion and hence, an increase of the variance promotes an increase of forcing energy. Figure 7(a) also illustrates the kind of behavior presented by the system in phase space (blue). Note that lower vibration amplitudes (with oscillations around only one SEP) occur for $0.2 < \sigma < 0.4$. After that, a transition region (hatched) is observed, $0.4 < \sigma < 0.6$. When $\sigma > 0.6$, a different kind of behavior is obtained, where the system oscillates around multiple SEP and higher amplitudes are obtained. Note that when oscillation

amplitudes become greater ($\sigma > 0.6$), there is an increase of harvested energy, PS_v.

5. Combination of Harmonic and Random Excitation

After the analysis of pure harmonic and pure random excitations, this section presents the combination of both kinds of excitations. This analysis is representative of real energy harvesting systems since random excitations can represent either unavailable noise or excitation variations. Different values of forcing amplitude and frequency are investigated, considering distinct levels of randomness. The analysis begins considering predominant harmonic excitation, with small NSR. The value of NSR is then increased until random excitation becomes predominant.

5.1. *Influence of the forcing amplitude*

Bifurcation diagrams are built in order to identify the influence of forcing amplitude on system response. Figure 8 presents diagrams for different

values of NSR using the same procedure employed to build the bifurcation diagram presented in Fig. 3. Figure 8(a) presents a weak combination of harmonic-random forcing (NSR = 0.01). It can be observed that the period-1 orbit keeps stable for a large range of forcing amplitude. By increasing NSR = 0.05, the periodic window related to a period-5 orbit is replaced by a chaotic behavior, as shown in Fig. 8(b). Figure 8(c) shows the response for NSR = 0.3. Under this condition, pink points fill a bigger region in the bifurcation region, representing a greater dispersion in Poincaré section. Nevertheless, the system presents the same qualitative behavior. Black points indicate that chaotic region is enlarged.

With NSR = 1 [Fig. 8(d)], the system response changes considerably. For values of $f_0 < 0.04$, bifurcation diagram identifies two coexistent behaviors that are symmetric, in both of them the beam tip oscillates around only one SEP. For values of $0.04 < f_0 < 0.085$, the behavior changes but there is still coexistent behavior, both oscillate around the two SEP. For higher values of f_0, there is only one behavior and system oscillates around both SEP.
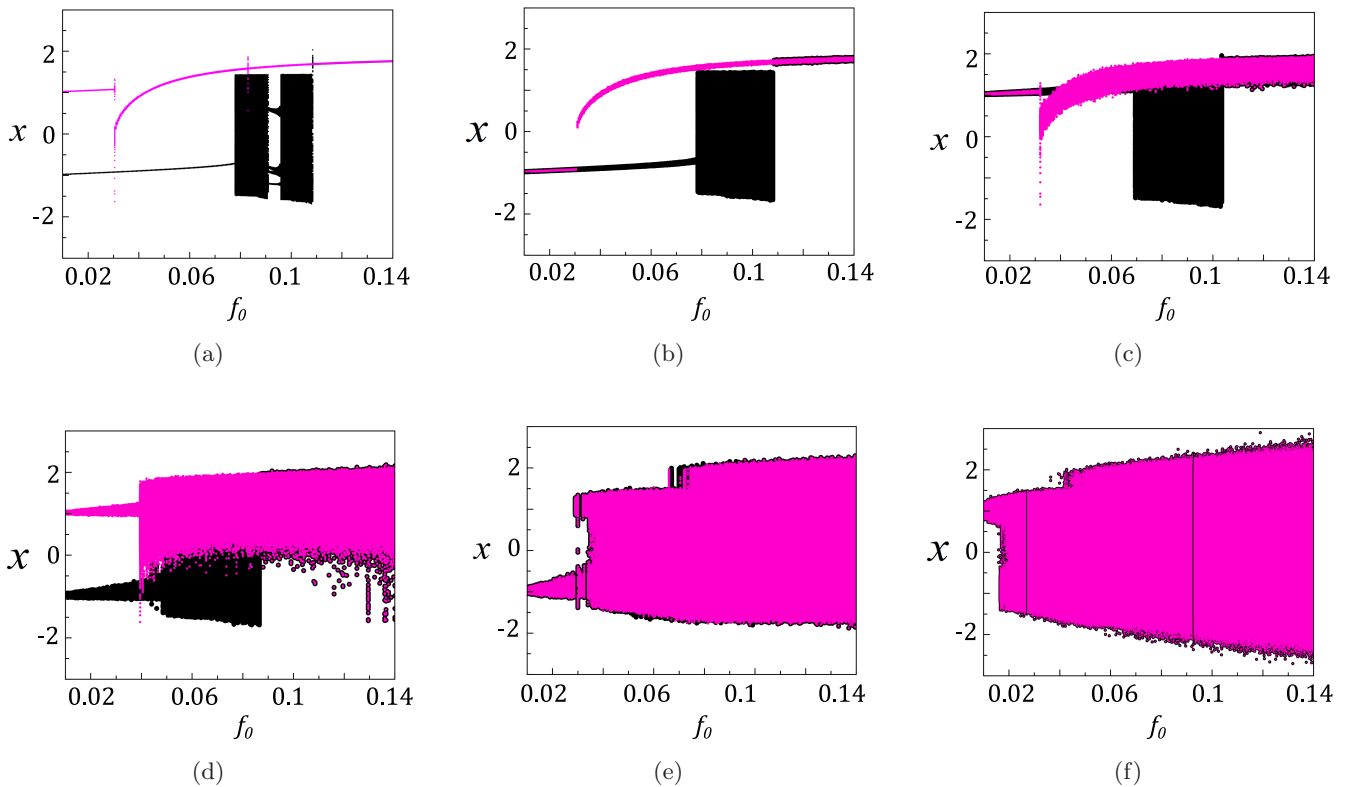

Fig. 8. Bifurcation diagram for different levels of combination of forcing and varying the amplitude. (a) NSR = 0.01, (b) NSR = 0.05, (c) NSR = 0.30, (d) NSR = 1, (e) NSR = 2 and (f) NSR = 5.

The coexistent behaviors, represented by black and pink colors, disappear when NSR = 2, as presented in Fig. 8(e). Under this condition, just two behaviors are observed: the system oscillates around only one SEP for smaller values of forcing amplitude; the system oscillates around multiple SEP for higher amplitudes, filling all phase space. For NSR = 5, the same result is obtained [Fig. 8(f)]. Based on that, it is possible to assume that random excitation is predominant for NSR ≥ 2.

5.2. *Influence of the forcing frequency*

The influence of forcing frequency on energy harvesting system response is now in focus. Figure 9 presents bifurcation diagrams with varying forcing frequencies and different NSR values. The same procedure of bifurcation diagram construction presented in Fig. 3(a) is adopted here. Pink points are related to a period-1 response obtained with initial conditions $(x_0, \dot{x}_0, v_0) = (1, 1, 0)$, while black points are related to chaotic behavior obtained with initial condition $(x_0, \dot{x}_0, v_0) = (1, 0, 0)$ with $f_0 = 0.083$ and $\omega = 0.8$. From these two coexisting attractors,

the forcing frequency is increased and decreased. These four procedures are plotted together in each diagram.

Figure 9 presents the bifurcation diagram for NSR = 0.01, this result is similar with the reference bifurcation diagram shown in Fig. 3(a). By increasing to NSR = 0.3 [Fig. 9(b)], a significant change occurs. Note that for $\omega < 0.78$ and $\omega > 1.3$, the system behavior related to pink and black points consists of oscillations around just one SEP. Note that there are two coexisting attractors, one has Poincaré section points around $x = -1$ and the other around $x = 1$. Thus, depending on the initial condition, the system oscillates around $x = -1$ or $x = 1$, which corresponds to two different behaviors. For $\omega > 0.5$, a similar behavior is observed to the one presented in Fig. 9(a), with pink points with a greater dispersion of the points in a response that oscillates around multiple SEP, while black points are related to chaotic behavior. Even in the presence of noise, the Poincaré section presents a lamellar structure. For NSR = 1 [Fig. 9(c)], the coexistence of behavior disappears, and two distinct behaviors are presented. For smaller values of forcing excitation all Poincaré section is filled with no pattern, as
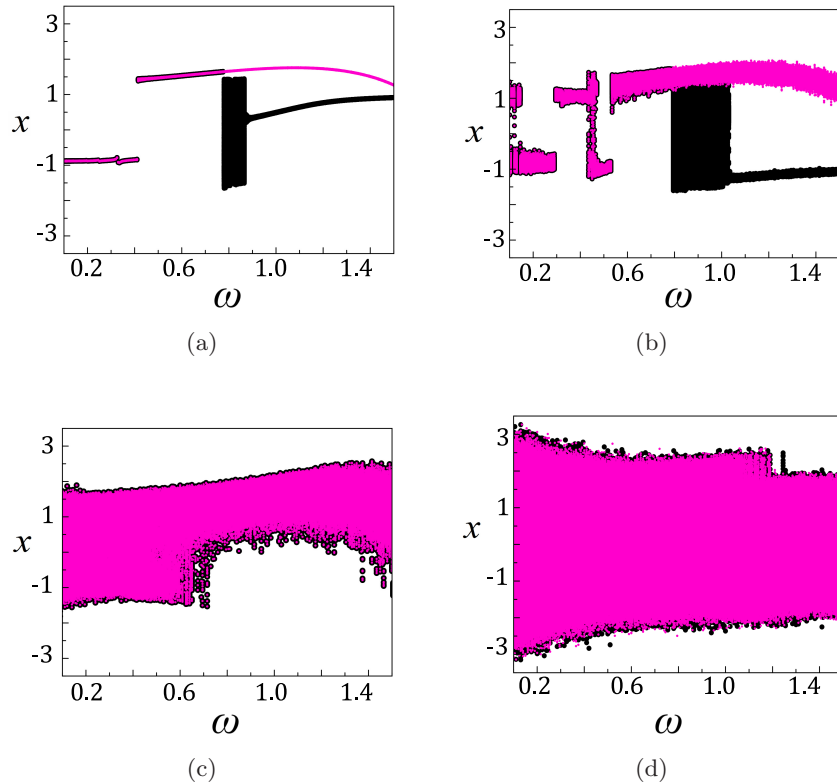

Fig. 9. Bifurcation diagram for different levels of combination of forcing and varying the frequency. (a) NSR = 0.01, (b) NSR = 0.3, (c) NSR = 1 and (d) NSR = 5.

well for the phase space. For higher values of f_0, the system oscillates around both SEP always with big oscillation amplitudes. When NSR = 5 [Fig. 9(d)], the same result is obtained. Once again, it is possible to assume that random excitation is predominant for NSR $\geq$ 1.

6. Energy Harvesting and Performance Analysis

This section aims to analyze the harvested energy and system performance. Four reference responses (identified when NSR = 0) are chosen: one chaotic orbit; two different period-1 orbits oscillating around multiple SEP; and one period-1 orbit oscillating around only one SEP. The dynamic evolution of these reference orbits is analyzed when NSR is increased.

The analysis of the first case, chaotic response, is presented in Fig. 10. Harmonic excitation

(a)

(b)

Fig. 10. System behavior when NSR is increased from 0 to 3 by considering the first reference orbit. (a) PS_f, PS_v and qualitative response of the system and (b) r.

parameters are $f_0 = 0.083$ and $\omega = 0.8$. By increasing NSR, after a transition region (hatched), the system presents a response that oscillates around multiple SEP with large amplitudes. This behavior presents the best performance and harvested energy as it can be observed from the values of PS_v and r. For values of NSR > 2, a different behavior is observed. Comparing this response with the chaotic one, the value of PS_v is greater but with a smaller r, once more mechanical energy is provided to the system as the noise increases.

Figure 11 presents details of the three behaviors identified in Fig. 10. Figure 11(a) shows a chaotic-like response in phase space and Poincaré section for NSR = 0.01. Figure 11(b) presents the response for NSR = 0.5, this kind of behavior occurs for $0.5 \leq$ NSR ≤ 1.5. Figure 11(c) shows the behavior for NSR = 5. Note that in the last case, the system oscillates without any pattern, filling all phase space, showing that random excitation is predominant. This kind of behavior occurs for NSR $\geq$ 2. Figure 12 shows the PSD curve for the three behaviors presented in Fig. 11.

The same analysis presented in Fig. 10 is now carried out for the second reference situation, period-1 orbit oscillating around multiple SEP, presented in Fig. 13, considering $f_0 = 1.4$ and $\omega = 0.1$. Values of PS and r are presented as a function of NSR, varying from 0 to 3. Figure 13(a) also illustrates the kind of behavior presented by the system in phase space (blue) together with Poincaré section (pink). Note that the reference response occurs until NSR = 1 and, after a transition region (hatched), a different type of behavior is obtained, where the phase space is all filled. It is important to highlight that the presented phase spaces and Poincaré sections are obtained for fixed values of
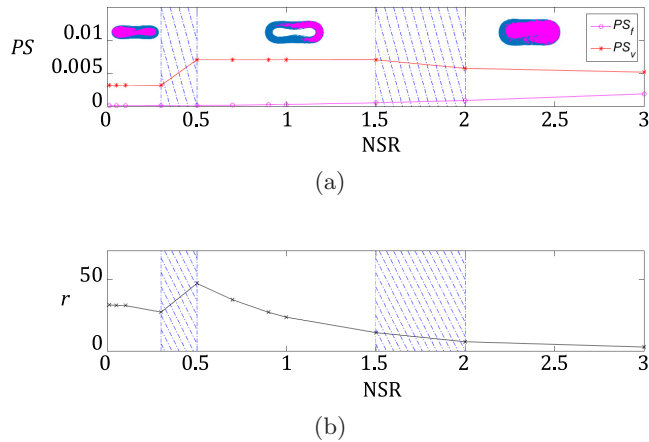
(a)

(b)

(c)
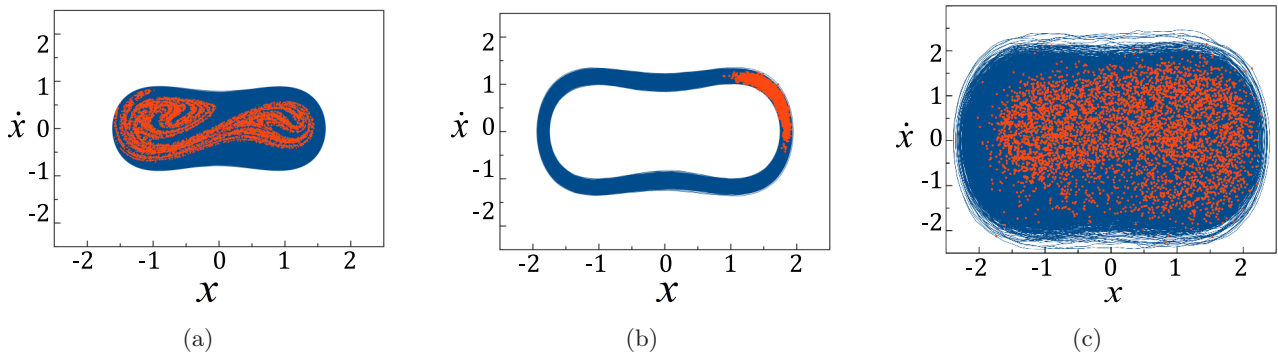
Fig. 11. Phase space (blue) and Poincaré section (red) for combined harmonic and random excitations with (a) NSR = 0.1, (b) NSR = 0.5 and (c) NSR = 5.
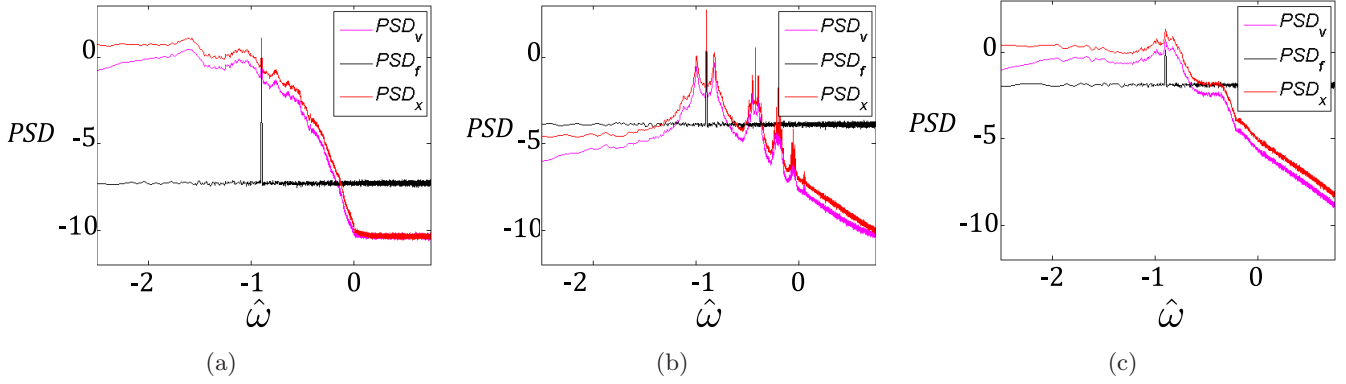
Fig. 12.   PSD curve for combined harmonic and random excitations with (a) NSR = 0.01, (b) NSR = 0.5 and (c) NSR = 5.
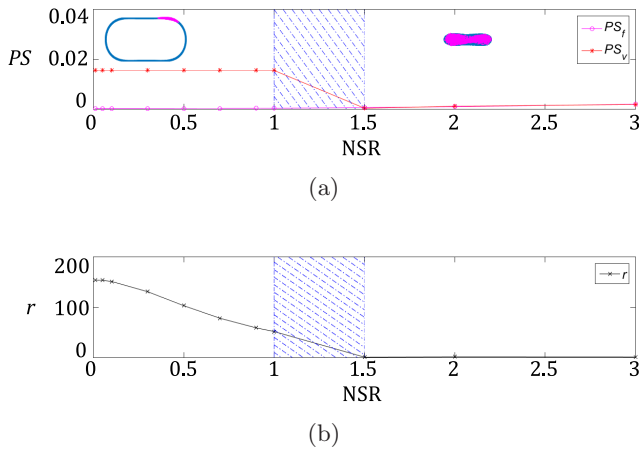

Fig. 13.   System behavior when NSR is increased from 0 to 3 by considering the second reference orbit. (a) PS_f, PS_v and qualitative response of the system and (b) r.

NSR, however, each one is used to represent the qualitative behavior presented by the system in a range of NSR. Note that the first region ($0 <$ NSR < 1) is more appropriated for energy harvesting due to higher value of PS_v. Moreover, by considering the value of r, the performance of the system is better for smaller values of NSR.

The same analysis is now carried out for the third reference situation, a period-1 orbit oscillating around both SEP, as presented in Fig. 14. This reference orbit has lower oscillation amplitude when compared to the second reference orbit. Harmonic forcing parameters are $f_0 = 0.1$ and $\omega = 0.8$. Note that the second reference orbit (Fig. 13) has better performance and it is more suitable for energy harvesting than this third orbit. This is due to the higher oscillation amplitudes of the first reference orbit. From Fig. 14, it can be observed that the first region is better for energy harvesting, PS_v, and presents the best performance, r. In

the interval from NSR = 0.3 to NSR = 0.5 emerges a behavior that oscillates around just one SEP that is not convenient for energy harvesting purpose. For NSR > 0.7, the system oscillates without any
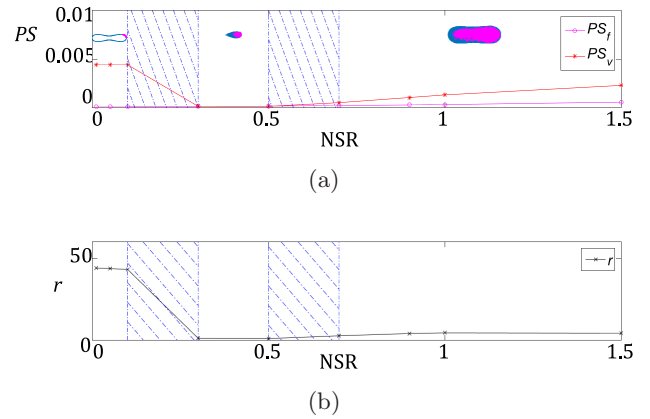

Fig. 14.   System behavior when NSR is increased from 0 to 1.5 by considering the third reference orbit. (a) PS_f, PS_v and qualitative response of the system and (b) r.
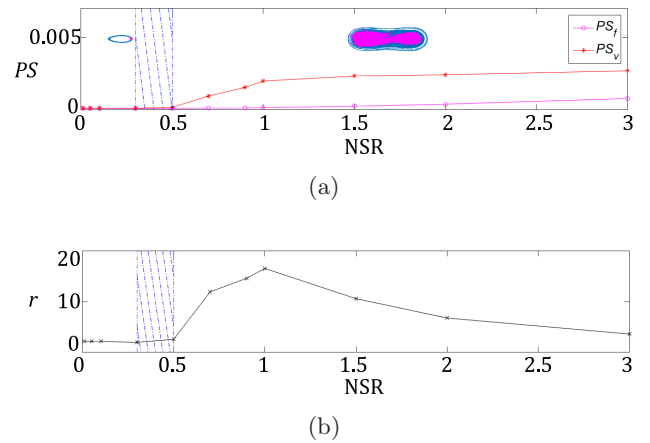

Fig. 15.   System behavior when NSR is increased from 0 to 3 by considering the last reference orbit. (a) PS_f, PS_v and qualitative response of the system and (b) r.

pattern, filling all phase space, as occurs in the case presented in Fig. 11(c).

Figure 15 presents the analysis of the last reference case. Harmonic forcing parameters are $f_0 = 0.063$ and $\omega = 0.8$. Note that the initial behavior is not appropriate to harvest energy, presenting the lowest PS_v and r of reference orbits. When $NSR = 0.5$, the system response changes, increasing both the harvested energy and system performance. For this case, the performance r achieves the best value when $NSR = 1$.

7. Conclusions

This paper deals with the random and nonlinear influence on energy harvesting. A bistable piezomagnetoelastic structure is evaluated considering three distinct excitations: pure harmonic, pure random and a combination of harmonic and random excitations. For the pure harmonic excitation, a rich dynamical response is observed. Nine cases are chosen to investigate the harvested energy and system performance. In this first analysis, one concludes that for energy harvesting purposes the best response is associated with trajectories presenting higher amplitudes. When the system is subjected to a random excitation, two types of responses are observed: vibrations around only one SEP and oscillations around both SEP. The best situation occurs for the smaller excitation variance that leads to oscillations around both SEP. By combining harmonic and random excitations, four reference orbits are chosen from the analysis of purely harmonic excited system ($NSR = 0$). From these four different behaviors, the system global dynamics is analyzed when NSR is increased, evaluating the harvested energy and system performance. The increase of NSR promotes qualitative changes in system response and more suitable responses for energy harvesting purposes are identified. The best behavior occurs when the tip of the beam oscillates around both SEP with the largest oscillation amplitude for the largest period. Moreover, proper combination of harmonic forcing parameters and NSR leads to this desired behavior. Based on that, it is possible to combine random and nonlinear effects in order to enhance energy harvesting capacity.

Acknowledgments

References

Abdelmoula, H., Zimmerman, S. & Abdelkefi, A. [2017] "Accurate modeling, comparative analysis, and performance enhancement of broadband piezoelectric energy harvesters with single and dual magnetic forces," *Int. J. Nonlin. Mech.* **95**, 355–363.

Cao, J., Zhou, S., Wang, W. & Lin, J. [2015] "Influence of potential well depth on nonlinear tristable energy harvesting," *Appl. Phys. Lett.* **106**, 173903.

Cheng, Y., Wu, N. & Wang, Q. [2017] "An efficient piezoelectric energy harvester with frequency self-tuning," *J. Sound Vibr.* **396**, 69–82.

Chiacchiari, S., Romeo, F., McFarland, D. M., Bergman, L. A. & Vakakis, A. F. [2017] "Vibration energy harvesting from impulsive excitations via a bistable nonlinear attachment," *Int. J. Nonlin. Mech.* **94**, 84–97.

De Paula, A. S., Inman, D. J. & Savi, M. A. [2015] "Energy harvesting in a nonlinear piezomagneto-elastic beam subjected to random excitation," *Mech. Syst. Sign. Process.* **54–55**, 405–416.

Erturk, A., Hoffmann, J. & Inman, D. J. [2009] "A piezomagnetoelastic structure for broadband vibration energy harvesting," *Appl. Phys. Lett.* **94**, 254102.

Feenstra, J., Granstrom, J. & Sodano, H. [2008] "Energy harvesting through a backpack employing a mechanically amplified piezoelectric stack," *Mech. Syst. Sign. Process.* **22**, 721–734.

Ferrari, M., Baù, M., Guizzetti, M. & Ferrari, V. [2011] "A single-magnet nonlinear piezoelectric converter for enhanced energy harvesting from random vibrations," *Sensors and Actuators A*: *Phys.* **172**, 287–292.

Hou, Y., Wang, L., Wang, D., Yang, H., Guo, M., Ye, Z. & Tong, X. [2017] "A preliminary study on the IoT-based pavement monitoring platform based on the piezoelectric-cantilever-beam powered sensor," *Adv. Mater. Sci. Engin.* **2017**, 4576026.

Kim, P., Nguyen, M. S., Kwon, O., Kim, Y.-J. & Yoon, Y.-J. [2016] "Phase-dependent dynamic potential of magnetically coupled two-degree-of-freedom bistable energy harvester," *Scient. Rep.* **6**, doi:10.1038/srep34411.

Lallart, M., Anton, S. R. & Inman, D. J. [2010] "Frequency self-tuning scheme for broadband vibration energy harvesting," *J. Intell. Mater. Syst. Struct.* **21**, 897–906.

Leng, Y., Tan, D., Liu, J., Zhang, Y. & Fan, S. [2017] "Magnetic force analysis and performance of a tristable piezoelectric energy harvester under random excitation," *J. Sound Vibr.* **406**, 146–160.

Litak, G., Friswell, M. I. & Adhikari, S. [2010] "Magnetopiezoelastic energy harvesting driven by random excitations," *Appl. Phys. Lett.* **96**, 214103.

Litak, G. [2014] "Energy harvesting by coupled oscillators forced by excitations with harmonic and random components," *Proc. Appl. Math. Mech.* **14**, 289–290.

Litak, G., Friswell, M. I. & Adhikari, S. [2016] "Regular and chaotic vibration in a piezoelectric energy harvester," *Meccanica* **51**, 1017–1025.

Mann, B. P. & Sims, N. D. [2009] "Energy harvesting from the nonlinear oscillations of magnetic levitation," *J. Sound Vibr.* **319**, 515–530.

Moon, F. C. & Holmes, P. J. [1979] "A magnetoelastic strange attractor," *J. Sound Vibr.* **65**, 275–296.

Newland, D. E. [1993] *An Introduction to Random Vibrations, Spectral and Wavelet Analysis* (Longman Scientific & Technical).

Oumbé Tékam, G., Kitio Kwuimy, C. & Woafo, P. [2015] "Analysis of tristable energy harvesting system having fractional order viscoelastic material," *Chaos* **25**, 013112.

Pereira, T., De Paula, A., Fabro, A. & Savi, M. [2017] "Energy harvesting in a nonlinear system under harmonic and random excitations," *Proc. 6th Int. Conf. Computational Methods in Structural Dynamics and Earthquake Engineering* (*COMPDYN 2015*) (Rhodes Island, Greece), pp. 459–469.

Rome, L. C., Flynn, L., Goldman, E. M. & Yoo, T. D. [2005] "Generating electricity while walking with loads," *Science* (*N.Y.*) **309**, 1725–1728.

Roundy, S. & Zhang, Y. [2005] "Toward self-tuning adaptive vibration-based microgenerators," *Proc. SPIE*, Vol. 5649, pp. 373–384.

Shenck, N. S. & Paradiso, J. A. [2001] "Energy scavenging with shoe-mounted piezoelectrics," *IEEE Micro* **21**, 30–42.

Silva, L. L., Savi, M. A., Monteiro Jr., P. C. & Netto, T. A. [2013] "Effect of the piezoelectric hysteretic behavior on the vibration-based energy harvesting," *J. Intell. Mater. Syst. Struct.* **24**, 1278–1285.

Silva, L. L., Savi, M. A., Monteiro, P. C. & Netto, T. A. [2015] "On the nonlinear behavior of the piezoelectric coupling on vibration-based energy harvesters," *Shock Vibr.* **2015**, 739381.

Sohn, J., Choi, S. B. & Lee, D. [2005] "An investigation on piezoelectric energy harvesting for mems power sources," *Proc. Instit. Mech. Engin. Part C*: *J. Mech. Engin. Sci.* **219**, 429–436.

Triplett, A. & Quinn, D. D. [2009] "The effect of non-linear piezoelectric coupling on vibration-based energy harvesting," *J. Intell. Mater. Syst. Struct.* **20**, 1959–1967.

Zhou, S., Cao, J., Inman, D., Liu, S., Wang, W. & Lin, J. [2015] "Impact-induced high-energy orbits of nonlinear energy harvesters," *Appl. Phys. Lett.* **109**, 093901.

Zhou, S., Cao, J., Inman, D., Lin, J. & Li, D. [2016] "Harmonic balance analysis of nonlinear tristable energy harvesters for performance enhancement," *J. Sound Vibr.* **373**, 223–235.